LBL--13698

DE83 003282 LBL-13698

Conf-811088--6

Lawrence Berkeley Laboratory

UNIVERSITY OF CALIFORNIA

Materials & Molecular Research Division

Presented at the 34th Pacific Coast Regional Meeting of the American Ceramic Society, Newport Beach, CA, October 25-28, 1981

PROCEDURE FOR ANALYZING THE X-RAY LINE PROFILES OF DISORDERED CARBONS

Leo G. Henry, R.H. Bragg, and S. Bose

December 1981

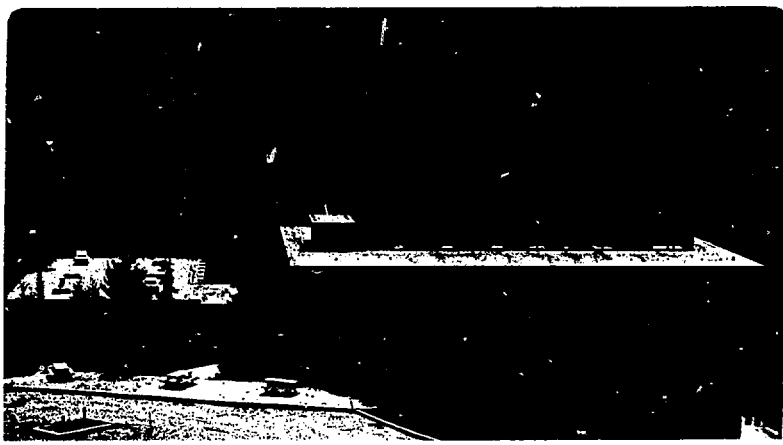

MASTER

DISTRIBUTION OF THIS DOCUMENT IS UNLIMITED

Prepared for the U.S. Department of Energy under Contract DE-AC03-76SF00098

LBL-13698

Presented at the 34th Pacific Coast Regional Meeting of the American Ceramic Society, October 25-28, 1981, Newport Beach, California

PROCEDURE FOR ANALYZING THE X-RAY LINE PROFILES OF DISORDERED CARBONS

Leo G. Henry, R. H. Bragg and S. Bose

December 1981

DISCLAIMER

Prepared for the U.S. Department of Energy under Contract No. DE-AC03-76SF00098

DISTRIBUTION OF THIS DOCUMENT IS UNLIMITED

PROCEDURE FOR ANALYZING THE X-RAY LINE PROFILES OF DISORDERED CARBONS

Leo G. Henry, R. H. Bragg and S. Bose

Materials and Molecular Research Division, Lawrence Berkeley Laboratory and
Department of Materials Science and Mineral Engineering,
University of California
Berkeley, CA 94720

ABSTRACT v

1. INTRODUCTION 1

2. THEORY 3

A. General 3

B. Irradiated Volume 4

C. Air Scattering and Resolving Time 5

D. Low Specimen Absorption 6

E. Compton's Incoherent X-ray Scattering (CIXS) 9

F. Small Angle X-ray Scattering (SAXS) 10

G. Lp, f^2 and ABS(2θ) Factors 12

3. EXPERIMENTAL PROCEDURE 13

4. PROCEDURE FOR CORRECTIONS 14

5. RESULTS 15

6. DISCUSSION 17

7. CONCLUSIONS 19

REFERENCES, FIGURES, FIGURE CAPTIONS 21

ACKNOWLEDGEMENT 24

FIGURE CAPTIONS 25

FIGURES 26

PROCEDURE FOR ANALYZING THE X-RAY LINE PROFILES OF DISORDERED CARBONS

Leo G. Henry, R. H. Bragg and S. Bose

Materials and Molecular Research Division, Lawrence Berkeley Laboratory and
Department of Materials Science and Mineral Engineering
University of California
Berkeley, CA 94720

ABSTRACT

A systematic procedure to correct for various distortions in the broad x-ray line profiles of glass-like carbons (GC) is described. The profile is first corrected for distortions due to low specimen absorption, secondly for incoherent (Compton) scattering, and then strong small angle scattering. The resulting profile is then multiplied by the appropriate trigonometric (Lorentz and polarization) factors. Finally, correction is made for the variation of the atomic scattering factor across the broad peaks. Two examples of the GC heat treated at 1000°C and 2700°C have been used to illustrate the outcome of the corrections.

1. INTRODUCTION

X-ray diffraction (XRD) line profiles from crystalline materials are fairly simple to analyze and the experimental procedure has been standardized (1). However, materials which do not give sharp peaks pose some problems. Examples abound. Silica gel gives a broad and diffuse peak which is asymmetric due to the strong contribution of small angle scattering. The peak is broad presumably because silica gel is amorphous. Clays, however, are highly crystalline but sometimes give broad peaks because of small crystallized sizes. Glass-like carbons (GC), a nongraphitizable member of the carbon family, also belongs to this category. The diffraction pattern is characterized by broad, symmetric 001 peaks and asymmetric hk bands superimposed on a high background which is almost all incoherent at very large angles (2). Frequently, the intensity in the very low angle region increases rapidly and continuously as the scattering angle is decreased (3-11). It does not appear to be generally recognized that this very strong small angle x-ray scattering (SAXS) in GC makes an appreciable contribution to the intensity even at the position of the first interference maximum, that is, the 002 peak. In the course of our investigation of the kinetics of structural evolution with heat treatment of GC, it was found that corrections not normally required were necessary for this material and a standardized procedure for obtaining distortion free line profiles would be useful. Before an analysis of the pattern in terms of the contributions of particle size, strain, and other defects to the broadening of the line profiles can be made, small angle scattering and background components must be removed. But even prior to this, two additional sources must be eliminated: when using reflection geometry the x-ray beam penetrates the GC samples to an appreciable depth causing a displacement of the x-ray

patterns towards smaller angles, and the use of flat samples of finite length combined with slit collimated divergent beams introduces a variable irradiated volume and a departure from focusing conditions. It was found that interplanar spacing and crystallite sizes determined from the uncorrected as-recorded x-ray patterns are erroneous, sometimes as much as 10% and 50% respectively. Errors in these parameters obviously are transferred to errors in kinetic parameters derived from the data.

The manner in which the foregoing factors distorts the diffraction patterns of these glass-like carbons will be discussed and procedures to effect the necessary corrections will be demonstrated using data obtained from two samples heat treated at 1000°C for 1 hour and 2700°C for 2 hours.

The objective of this paper then is to show how to obtain data which warrant analysis only; no attempt is made to conduct an analysis of the corrected data in terms of any model of defect structure. It must be noted, however, that the above method is applicable to data collected by powder diffractometry.

2. THEORETICAL

A. General

For polycrystalline samples with broad reflections the observed intensity I_{obs}, diffracted at any angle 2θ can be written as:

$$I_{obs}(2\theta) = [C_1.Lp.ABS(2\theta).f^2.I_g(2\theta)]+I_b(2\theta)+I_{saxs}(2\theta)+I_{air}(2\theta) \quad (1)$$

where C_1 is a constant (to be defined later); $Lp=[(1+\cos^2 2\theta)/\sin\theta)]$ is the modified Lorentz Polarization factor (12); $ABS(2\theta)=[1-\exp(-2\mu T/\sin\theta)]$ is the absorption factor for reflection geometry with μ=linear absorption coefficient and T=thickness of the sample (for transmission, $ABS(2\theta) = [\exp(-\mu T/\cos\theta)]$; f^2 is the square of the atomic scattering factor; $I_b(2\theta)$ is the background intensity; $I_{saxs}(2\theta)$ is the small angle x-ray scattering (SAXS) intensity, [the tail extends to large 2θ angles due to microporosity ($\sim$30Å in diameter) in GC]; $I_{air}(2\theta)$ is the intensity due to air scattering (13,14), and $I_g(2\theta)$ is the corrected interference line profile which contains the desired information such as d-spacings, crystallite size and strain broadening, and lattice defects.

B. Irradiated Volume

The use of reflection geometry requires an extremely long sample when obtaining data in the small angle region. In addition, theory assumes the use of a parallel beam so a divergent beam contributes to distortion of the data.

The experimental situation is as seen in Fig. 1. The divergent beam and reflection geometry cause the incident x-ray beam to miss the sample first on the left edge (OX side) when $L/2=[R\ \mathrm{Sin}\alpha/\mathrm{Sin}(\theta-\alpha)]$ and then on the right edge (OY side) when $L/2=[R\ \mathrm{Sin}\alpha/\mathrm{Sin}(\theta+\alpha)]$. Typically $L=5.00$cm, $R=14.55$cm, so for $2\alpha=1°$, then $2\theta=6.82$ and $4.82°$ respectively.

The assumption that a parallel beam of area A_0 is used provides for an irradiated length of sample given by $A_0/\mathrm{Sin}\theta$. Since experimentally we use a divergent beam, then the area becomes $2R\mathrm{Tan}\alpha$ and the irradiated length becomes equal to $[R\mathrm{Sin}\theta\mathrm{Sin}\ 2\alpha/\mathrm{Sin}(\theta-\alpha)\mathrm{Sin}(\theta+\alpha)]$.

It is easy to show then that the corrected intensity I_{corr} for beam spill on one side (OX) is given by

$$I(2\theta)_{corr} = I(2\theta)_{obs} \times \frac{\mathrm{Sin}(\theta+\alpha)}{[\ell_0 x\mathrm{Sin}(\theta-\alpha)+R\mathrm{Sin}\alpha]} \times \frac{2R\mathrm{tan}\alpha}{\mathrm{Sin}\theta} \qquad (2)$$

and both sides by

$$I(2\theta)_{corr2} = I(2\theta)_{obs} \times [\frac{1}{2\ell_0} \times \frac{2R\mathrm{tan}\alpha}{\mathrm{Sin}\theta}] \qquad (3)$$

Using $2\theta=1.0°$, the correction factor for $2\ell=5.00$cm increased from 1.02 at at $2\theta=5.8°$ to 5.06 at $2\theta=1.5°$. Based on the above, the corrected SAXS data for reflection gave profiles which were parallel to that obtained using transmission geometry.

C. Correction for Air Scattering and Resolving Time

The angular distribution of the intensity scattered from air is continuous and decreases with increasing $\sin\theta/\lambda$(1). This air scattering may be largely eliminated by providing a helium-filled or vacuum path for the primary and scattered x-rays (15) or a geometrical correction may be applied (14). With regard to the second method which was employed in this work, the relationship between the scattering from an air volume in the absence of a specimen and when a flat speciman of thickness T is inserted is given by

$$a_R = \frac{1}{2} + \left(\frac{1}{2} - \frac{T\cos\theta}{R\beta}\right)\exp(-2\mu T/\sin\theta) \qquad (4)$$

and

$$a_T = \left(1 - \frac{T\sin\theta}{R\beta}\right)\exp(-\mu T/\cos\theta) \qquad (5)$$

where a_R and a_T represents the ratio of the air-scattered intensity received with and without the sample in place for reflection and transmission geometries respectively; β is the equatorial angle subtended at the specimen by the detector slit, and R is the goniometer radius. The magnitude of the air scatter with the specimen in place is obtained by measuring the air scattering in the absence of the specimen and multiplying the result by the appropriate equation.

The correction for counting losses (1) due to resolving time in scintillation and proportional counters is necessary at extremely low angles where the counter fails to register all photons entering the detector resulting in nonlinear detector response. Bragg (16) and Short (17) have shown that it is possible to determine nonlinearity correction for any type of x-ray counter with the use of multiple foils and with only one foil respectively. The first method is adopted in the work reported here.

D. Correction for Low Specimen Absorption

It has been shown by Keating and Warren (18) and later by Bragg and Packer (19) that if $I_g(2\theta)$ is the true line profile, then the observed line profile $I(2\theta)$ is given by

$$I_R(2\theta_m) = \frac{A_o R}{\sin 2\theta_m} \int_{2\theta_m}^{2\theta_m + 2T\cos\theta_m/R} \exp\left[\frac{2\mu R}{\sin 2\theta_m}(2\theta_m - 2\theta)\right] \cdot I_g(2\theta)\, d2\theta \qquad (6)$$

for reflection and

$$I_T(2\theta) = \frac{A_o R}{\sin 2\theta_m} \exp\left[-\frac{\mu T}{\cos\theta_m}\right] \int_{2\theta_m}^{2\theta_m + 2T\sin\theta_m/R} I_g(2\theta)\, d2\theta \qquad (7)$$

for transmission where $2\theta_m$ is the measured angle; 2θ is the true angle. A_o is the cross-sectional area of the incident beam, R is the source-specimen and specimen-detector slit distance, μ is the linear absorption coefficient, and T is the thickness of the specimen. Procedures for correcting the observed intensity data, $I_{obs}(2\theta)$ for low specimen absorption in order to obtain $I_g(2\theta)$ are given in references (18) and (19). The equation for applying the correction to the symmetrical reflection geometry is

$$K \frac{A_o}{2\mu} I_g(2\theta_m) + I_{bas}(2\theta) = \left[I_{obs} - \frac{I'}{\gamma_R}\right]_{2\theta} + \left[I_{obs} - \frac{I'}{\gamma_R}\right]_{2\theta + U_R} \cdot \exp(-\gamma_R U_R) \qquad (8)$$

where $I' = dI(2\theta)/d(2\theta)$ and $d(2\theta)$ is expressed in radians; $\gamma_R = 2\mu R/\sin 2\theta$; $U_R = 2T\cos\theta/R$; K is some constant, and the other terms A_o, μ, R, and T are defined before; and $I_{bas}(2\theta)$ represents the sums of the air, saxs and background scattering. In Eq. (8), we see that for $\gamma_R U_R > 5$, the series converges so rapidly

that only the first term suffices. For the GC specimens used here $\gamma_R U_R$ ranged from 5.8 at $2\theta = 40°$ to 229 at $2\theta = 1.0°$ so only the first term was used to correct the 002 peak. Thus Eq. (8) reduces to

$$\left[I_{obs} - \frac{I}{\gamma_R}\right] = K \frac{A_o}{2\mu} I_g(2\theta) + I_{BAS}(2\theta) \qquad (9)$$

A qualitative assessment of the distortion can be obtained by first noting that it is convenient to choose the specimen thickness such that $T=1/\mu$. Since for GC materials μ is large (of the order of 5-7cm^{-1}) then Eqns. (6) and (7) reduce to

$$I_R(2\theta_m) = \frac{A_o}{2\mu} [1-\exp(-\frac{2\mu T}{\sin\theta_m})] \cdot g(2\theta_m) \qquad (10)$$

and

$$I_T(2\theta_m) = \frac{A_o T}{\cos\theta_m} \exp[-\mu T/\cos\theta_m] \cdot g(2\theta_m) \qquad (11)$$

These are the well known expressions for the intensity in the reflection and transmission cases. This choice provides maximum diffraction efficiency from small angle scattering for transmission, and calculations using these two equations show that the diffraction efficiency in transmission and in reflection remain remarkably constant and close to unity as 2θ decreases and has only dropped to 91% and 94% respectively at $2\theta = 90°$. Further, a check on the ratio of the transmission to the reflection I_T/I_R under the same conditions of $T = 1/\mu$ produces

$$\frac{I_T}{I_R} = \frac{2}{\cos\theta} \times [\frac{\exp(-1/\cos\theta)}{1-\exp(-2/\sin\theta)}] \qquad (12)$$

This ratio is $\approx \frac{2}{e} = 0.74$ at $2\theta = 0°$ and reduces only to 0.71 at $2\theta = 90°$. All other factors being equal for transmission and reflection, this provides a check and confirmation that the material is isotropic on the macroscopic scale.

The form of Eqns. (6) and (7) indicates that the diffraction pattern will be displaced towards smaller angles 2θ (Fig.3) and the displacement will be of the order of $(T\sin\theta_m/R)$. For GC for which $\mu T=1.00$, and $T\sim0.16$cm, the displacement is of the order of $0.63\sin\theta_m$. For example, at the position of the 002 line of the turbostratic carbons, $d\sim3.44$Å, and $2\theta = 26.6°$, therefore $\Delta2\theta\approx0.30°$. Using these procedures, Henry and Bragg (20) found that for the GC samples investigated, the shift of the 002 peak is significant enough to warrant correction.

E. Compton's Incoherent X-ray Scattering (CIXS)

The intensity of the Compton incoherent x-ray scattering from the GC samples can be measured directly (21) or determined by comparison (2) with the incoherent x-ray scattering from very large grain size pyrolytic graphite (PG). It has already been shown (2) that both methods give essentially the same result. In this work, the second method is employed. It is based on (i) the fact that the background in crystalline carbon samples, example PG is essentially all incoherent scattering except near an intensity maximum and (ii) on the demonstration that the effective volume for coherent and incoherent scattering are equal (19). The measured incoherent intensities in PG and GC were obtained according to (2) and that in GC was also obtained from that measured in PG using the following ratio

$$\frac{I_{INC}^{GC}(2\theta)}{I_{INC}^{PG}(2\theta)} = \frac{k_{GC}}{k_{PG}} \times \frac{[1-\exp(-2\mu_s T_s)/\mathrm{Sin}\theta)]_{GC}}{[1-\exp(-2\mu_s T_s)/\mathrm{Sin}\theta)]_{PG}} \times \frac{[1-\alpha(2\theta)]_{GC}}{[1-\alpha(2\theta)]_{PG}} \qquad (13)$$

where $k = \rho/2\mu_s$, ρ being the samples density, μ_s, the linear coherent absorption coefficient, T the samples thickness, and $\alpha(2\theta)$ is the correction due to the differential absorption of the Compton scattering in the specimen, the air, and the beryllium counter. (22,23).

F. Correction for Small Angle X-ray Scattering (SAXS)

The data is corrected for SAXS by first plotting on a log-log scale the intensity $I_{saxs}(h)$ versus the scattering vector h ($=4\pi \sin\theta/\lambda$) using the small angle portion of the diffraction pattern. Theoretically, the Porod asymptotic law (24) can be written as

$$I_{saxs}(h) = I_c(h)\rho^2 2\pi S/h^n \qquad (14)$$

where S is the surface area, $I_0(h)$ is the incident beam, and ρ, the density of the material. It can be shown that for a large class of materials n=-4 for point collimation but for infinite slit collimation n=-3. A more exact calculation shows that (4) for slit collimation we can write

$$\lim h^3 J(h) = \frac{h^4}{2\beta} \cdot I(h) \cdot \tan^{-1}\left(\frac{2\beta}{h}\right) \qquad (15)$$

where $2\beta = 2\pi b/R\lambda$, b = slit height, β = soller slit divergence (vertical) and J(h) is the slit collimated intensity. It has been shown (25) that for a GE XRD5 with collimation of 0.4°MR in the incident beam, a second 0.4°MR after the sample and a 0.5° detector slit, then $J(h) \approx I(h)$ when $2\beta < h$. This condition exists for $2\theta > 0.40°$ for CuK_α radiation and is quite suitable for pore size measurements in the GC samples. Beyond this region $J(h) \approx I(h) \propto h^{-4}$. From the linear portions of the curves which are continuous, the small angle intensities, $I_{saxs}(h)$ at various angles can be determined using the following relation

$$I^{calc}_{saxs}(h) = \left[\frac{I_{SAXS}(h_1)}{h_1^n}\right] \times h^n$$
$$= \text{constant} \times h^n$$

where the constant is determined from the linear portion of the curve. Once the power is established, then I_{saxs}^{calc} at all other h values can be determined. This then is subtracted from the profile.

G. Lp f^2 and ABS(2θ) Factors

The modified Lorentz polarization Lp and the atomic scattering factor f are dependent on angular position, but the absorption factor ABS(2θ) depends also upon the μT of the particular material. For reflection,

$$ABS_R(2\theta) = [1-\exp(-2\mu T/\mathrm{Sin}\theta]) \tag{18}$$

and for transmission,

$$ABS_T(2\theta) = \exp(-\mu T/\mathrm{Cos}\theta) \tag{19}$$

The modified Lorentz polarization here is $Lp(2\theta) = [(1-\mathrm{Cos}^2 2\theta)/\mathrm{Sin}^2\theta]$ because it pertains to the line profile analysis, and for this reason the $(1/\cos\theta)$ term which relates to the line breadth (12) is dropped.

3. EXPERIMENTAL PROCEDURE

Two samples of glass-like carbons* heat treated in an inert atmosphere to 1000°C for one hour (GC1000-1) and 2700°C for two hours (GC2700-2) were cut into plates of nominal areas (2.5 x 5.0cm^2) and reduced to thicknesses about 0.16cm, which gave maximum diffraction efficiency in transmission. Density measurements on the bulk samples by (i) pyconometry using water N_2,He and kerosene, (ii) x-ray μt measurement, and (iii) by straightforward calculation using the measured mass and volume (LxBxH) were all in agreement. The values ranged from ρ=1.3-1.5 gm/cm^3.

The WAXD experimental data were obtained with a General Electric XRD5 diffractometer operating a nickel filtered copper tube at 45 kV and 35 mA in conjunction with pulse height discrimination. The collimation was 1° source, HR Soller, and 0.1° detector slits. The samples (5x2.5x0.16cm^3) were scanned in reflection in the range 2θ=1.0-160° with goniometer speed = 0.2° 2θ per min., chart speed ≈ 0.06" per min., and time constant = 0.5 sec.

*Obtained from Polycarbon, Inc., North Hollywood, CA., and prepared according to a process developed in the research laboratory of Lockheed Missiles Space Company.

4. PROCEDURE FOR CORRECTIONS

Because the raw data is collected using the reflection geometry, the data is first corrected for change in irradiated volume, for resolving time (counting losses) and air-scattering all of which are dominant at the very low angles ($\leq 5°$). In addition to reducing the intensity of the XRD lines, low specimen absorption also distorts the profile. This distortion is included in Eqn. (8) and is next to be corrected. The next step, that of removing the Compton incoherent scattering, can be accomplished by either of two methods (2). The second method is used in this analysis, after which the incoherent scattering is subtracted from the profile. When the distortions contributed by the factors discussed above have been removed, the x-ray pattern still contains the superposition of the SAXS and the WAXD. The removal of the former can be accomplished by first extrapolating ([25]) the data according to the appropriate h^n law, then subtracting the resulting continuous profile from the WAXD data. Finally, the effects of the angular variation of f^2 and Lp and the absorption are corrected for.

5. RESULTS

The uncorrected intensity profiles and the generated Compton incoherent curves for both GC specimens are shown in Fig. 2. The results of the corrections for irradiated volume, nonlinear counter response (resolving time) and low specimen absorption are given in Fig. 3 where we observe a shift in the 002 peak profile towards higher angles from 2θ = 25.5° to 25.7 for GC2700-2 and from 2θ = 23.5° to 24.1° for GC1000-1. The measured Compton incoherent scattering and the wide angle x-ray diffraction (WAXD) profile for PG at large 2θ are plotted in Fig. 4. In Fig. 5 it is seen that the non-Bragg (continuous) scattering in the small angle region follows the h^n Porod law for which $n \cong -3$ to -3.6. It is seen also that the correction for beam spill when using reflection geometry produces data which is parallel to that obtained in transmission. The subsequent corrections for Lp, ABS(2θ) and f^2, which converts the data in Fig. 2 to those in Figs. 6 and 7 have produced a transformation in the shape of the profiles as well as a further displacement of the peak position.

The parameters of the GC microstructure were calculated from the (002) and (10) maxima positions and full width at half maximum β, using the following relationships (29):

$$L_c = \frac{0.97\lambda}{\beta_c(\frac{1}{2},2\theta)\cos\theta_c} \quad \text{and} \quad L_a = \frac{1.77\lambda}{\beta_a(\frac{1}{2},2\theta)\cos\theta_a} \qquad (20a,b)$$

where L_a and L_c are the dimensions of the defect-free distances parallel to and perpendicular to the layer planes; λ is the wavelength; and θ the the Bragg angle. It is to be noted here that for the GC1000-1, L_a was

calculated using the peak breadth at the two-thirds maximum position because the latter is much less influenced by the (004) reflection which occurs on the high angle side of the (10) maxima. The relevant equation (26) is

$$L_a = \frac{0.94\lambda}{\beta_a(\frac{2}{3},2\theta)\mathrm{Cos}\theta_a} \tag{21}$$

The microstructural parameters of d_{002}, d_{10}, d_{004}, L_a and L_c are summarized in Table 1.

TABLE 1. MICROSTRUCTURAL PARAMETERS FOR TWO GLASSY CARBON SAMPLES

Lattice Parameters	GC2700-2			GC1000-1		
	Uncorrected	Corrected	% error	Uncorrected	Corrected	% error
$2\theta_{002}$	25.4°	25.9		23.6	25.8	
d_{002}	3.50Å	3.44Å	2%	3.77Å	3.45Å	9%
d_{10}	2.12Å	2.11Å	1%	2.09Å	2.08Å	1%
d_{004}	1.73Å	1.72Å	1%	Not resolved	1.69Å	—
L_c	22Å	25Å	12%	11Å	12Å	4%
L_a	58Å	87Å	33%	27Å	34Å	29%

6. DISCUSSION

When the profile is corrected for beam spill and beam divergence, we obtain a Porod dependence of -4.0 and -3.5 for GC2700-2 and GC1000-1 respectively. This is compared to values of -3.2 and -2.7 respectively before the correction. The low value of n for GC1000-1 even after correction is a consequence of (i) the differences in the electron density in the solid phase in GC heat treated to temperatures $\leq$ 2000°C (30), and (ii) the additional scattering due to the anisotropic density fluctuation in the carbon material (5,10). It has been shown (8) that these fluctuations decrease with increasing heat-treatment temperature. Figure 2 illustrates the intense nature of this small angle scattering compared to the first interference maxima (the 002 peak). The tail of this SAXS can be seen to have a modifying effect on the first maxima. That the removal of SAXS restores the shape of the profile has been demonstrated by Bose and Bragg (11) and by D'Antonio and Konnert (28). Figures 4 and 2 show the measured and generated curves respectively for the Compton scattering in both PG and GC. The differences were so small that they were superimposable. Subtraction of the CIXS and the SAXS strongly affects the line profiles but has little effect on peak positions. In respect of the latter, the largest contribution to the peak displacement as seen in Figs. 6 and 7 is that from the application of the correction for low specimen absorption.

The corrected line profiles, which represent the interference function for the GC samples, are shown in Figs. 6 and 7. Strikingly evident is the amount of detail revealed compared to that of Fig. 2 which is a plot of the raw data. Firstly, on both sides of the 002 reflection, the background has not only been reduced but the 002 peak has become more symmetrical.

Secondly, whereas in Fig. 2 the region around the hk (10) band is barely resolved, Fig. 6 clearly shows the 004 reflection quite distinct from the 10 reflection even for the GC1000-1 material (Fig.7). It is not expected that the tails of the peaks should go to zero between the maximas even after removal of background because of (i) the closeness of the peaks, and (ii) the extent of the particle size and strain broadening. In addition, amorphous or noncrystalline and paracrystalline materials scatter coherently at all angles making the notion of the intensity falling to a background level between discrete maxima quite inapplicable (1). It should now be noted that much of the asymmetry in the 002 peak shape disappears when the final corrections for f^2, L_p and Abs(2θ) are made (see Figs. 6 and 7). Also, no corrections for instrumental broadening were made since this would be quite small compared to the width of the narrowest peak.

7. CONCLUSIONS

The success of the procedure used can be inferred from the fact that all three maxima (002, 10 and 004) are clearly distinguishable. We note however, that the effect of strain which has not been removed, will be to render the integrated intensities of the 002, and 004 reflections unequal.

It can be seen that without corrections to the profile, investigators working with GC materials can overestimate d_{002} by as much as 0.32Å. When it is recalled that the range of d_{002} from turbostratic to completely graphitic carbons (3.44Å to3.35Å) is about 0.09Å it is clear that highly erroneous conclusions can be reached about the extent of the disorder of GC materials. The implication of these results are far reaching. It is probable that the range of structural disorder in hard carbons like GC is very similar to that in soft carbons like PG and that in the former the decrease in disorder attained for a given heat treatment is usually greater than that estimated from uncorrected profiles. Similar remarks apply to changes in L_a and L_c where it appears that these parameters have been greatly underestimated by as much as 30-40% for both low HTT (heat-treatment temperature) and HTt(heat-treatment time).

The microstructure of GC evident in high resolution micrographs (29,30 and Fig. 8), when combined with results from differential thermal expansion studies (31) indicates the presence of large frozen-in strains which the system is unable to relax even on heating to 3000°C. The effect of this strain is to add to the size broadening effect. In principle this component can be separated given a sufficient number of resolvable orders of a reflection, but as stated earlier no attempt at such analysis is made here.

The fully corrected line profiles then constitute the lattice interference function devoid of factors normally taken to be constant over the breadth of a Bragg reflection. These are the profiles which should be used in subsequent analyses such as for d-spacings, defect free distances (parallel and perpendicular to the layers), strain and shape. Hence, in order to obtain meaningful lattice parameters the x-ray line profiles of GC must be corrected for SAXS, CIXS and low specimen absorption in addition to the usual sources of line profile distortion.

REFERENCES

1. Klug, H. P. and L. E. Alexander, "X-ray Diffraction Procedures for Polycrystalline and Amorphous Materials," John Wiley, N.Y., 2nd Ed. (1974).
2. Henry, Leo G. and R. H. Bragg, Abstracts, 15th Biennial Carbon Conference, June 22-25, 1981, P 478, University of Pennsylvania, Philadelphia, PA. Manuscript to be submitted to Jour. Appl. Physics (1982).
3. Bragg, R. H., and M. L. Hammond, Abstracts, 7th Biennial Carbon Conference, June, 1965, Cleveland, OH; also Carbon, 3, 340 (1965).
4. Rothwell, W. S., Jour. Appl. Phys., 39, #3, 1840 (1968).
5. Perret, R., and W. Ruland, Jour. Appl. Cryst., 1, 308 (1968).
6. Perret, R., and W. Ruland, Abstracts, 10th Biennial Carbon Conference, June 27-July 2, LeHigh University, Bethlehem, PA., p.146 (1971).
7. Biswal, M. M., P. P. Bihuniak and R. H. Bragg, Abstracts, 10th Biennial Carbon Conference, June 27-July 2, Le High University, Bethlehem, PA., p.145 (1971).
8. Perret, R., and W. Ruland, Jour. Appl. Cryst., 5, 183 (1972).
9. Jenkins, R. G., and P. L. Walker, Jr., Abstracts, 11th Biennial Carbon Conference, June 4-8, Gatlinburg, TN., p.182 (1973).
10. Jenkins, R. G., and P. L. Walker, Jr., Carbon, 14, 7 (1976).
11. Bose, S., and R. H. Bragg, The 2nd International Conference on Carbon (Carbon '76), Deutsche Keramische Gesellschaft (German Ceramic Society), Baden-Baden, Federal Republic of Germany, p.205 (1976).
12. Cullity, B. D., "Elements of X-ray Diffraction," 2nd Ed., Addison Wesley Publ., Co., p.463 (1978).

13. Warren, B. E. and R. L. Mozzi, Jour. Appl. Cryst., 3, 59 (1970).

14. Ergun, S. in Chemistry and Physics of Carbon, Vol. 3 (P. L. Walker, Jr., Ed.) Marcel Dekker Publ. Co., NY, p. 225 (1968).

15. McCune, R. A. in Advances in X-ray Analysis, Vol. 6, Plenum Press, NY, p. 85 (1963).

16. Bragg, R. H. Rev. Sci. Instr., 28, 839 (1957).

17. Short, M. A. Rev. Sci. Instr., 31, 618 (1960).

18. Keating, D. T. and B. E. Warren, Rev. Sci. Instr., 23, 519 (1952).

19. Bragg, R. H. and C. M. Packer, Rev. Sci. Instr., 34, 1202 (1963).

20. Henry, Leo G. and R. H. Bragg, Abstracts, 14th Biennial Carbon Conference, June 25-29 (1979), p. 129. Penn State Univ., Univ. Park, PA.

21. Short, M. A. Acta Cryst., 14, 486 (1961).

22. McKinstry and M. A. Short, Proc. of 5th Carbon Conference, Vol. 2, p. 507 (1962).

23. McKinstry and M. A. Short, Z. für Kristall., 114, 278 (1960).

24. Guinier, A. and G. Fournet, "Small Angle Scattering of X-rays," John Wiley, NY p. 115 (1955).

25. Henry, L. G. and R. H. Bragg "SAXS in GC Using a GE XRD5 Soller Slit Collimated Diffractometer." Manuscript in prep; to be submitted to J. Appl. Cryst., (1982).

26. Warren, B. E. and P. Bodenstein, Acta Cryst., 20, 602 (1966).

27. Bose, S. and R. H. Bragg "Small Angle Scattering by Diffuse Interface," UCB-LBL 6656 (1977); manuscript submitted to J. Appl. Cryst. (1981).

28. D'Antonio, P. D. and J. H. Konnert, Abstracts, 15th Biennial Carbon Conference, June 22-26 (1981), p. 476, Univ. of Penn. Philadelphia, PA

29. Bose, S., U. Dahmen, R. H. Bragg and G. Thomas, Jour. Amer. Ceram. Soc., 61, p.174 (1978)

30. Bann, L. L. and W. M. Hess, Abstracts, 10th Biennial Carbon Conference, June 27-July 2,(1971), p. 161, Lehigh University, Bethlehem, PA.

31. Mehrotra, B. N. and R. H. Bragg, Abstracts, 15th Biennial Carbon Conference, June 22-26 (1981), p. 530, Univ. of Penn., Philadelphia, PA.

ACKNOWLEDGEMENT

This work was supported by the Director, Office of Energy Research, Office of Basic Energy Sciences, Materials Science Division of the U.S. Department of Energy under contract No. DE-AC03-76SF00098

FIGURE CAPTIONS

Fig. 1. Reflection geometry for beam spill and beam divergence.

Fig. 2. Uncorrected x-ray diffraction patterns of GC including small angle x-ray scattering (SAXS) and compton incoherent x-ray scattering (CIXS) profiles.

Fig. 3. Comparison between raw data and the low specimen absorption corrected profile.

Fig. 4. Comparison between Compton curves for PG and GC at large scattering vectors.

Fig. 5. Porod asymptotic curves in reflection and transmission for GC2700-2 and GC1000-1.

Fig. 6. Comparison between uncorrected and fully corrected line profiles for GX2700-2.

Fig. 7. Comparison between uncorrected and fully corrected line profiles for GC1000-1.

Fig. 8. Transmission electron micrograph of GC showing 00.1 planes of 3.4Å spacing resolved by lattice imaging technique (100kV tilted beam illumination). See also Ref. 29.

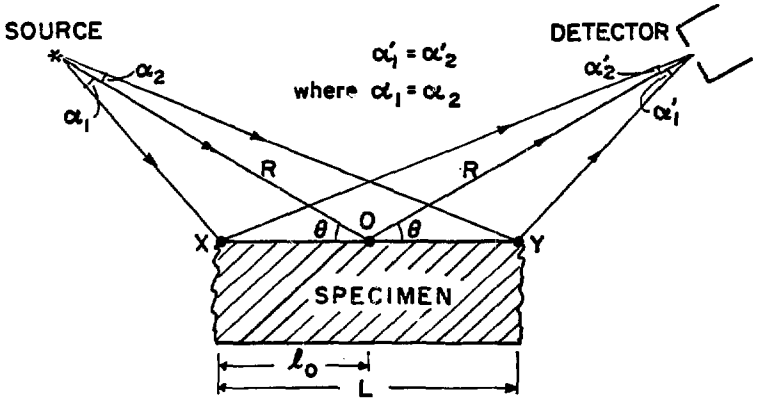

XBL829-6605

Fig. 1

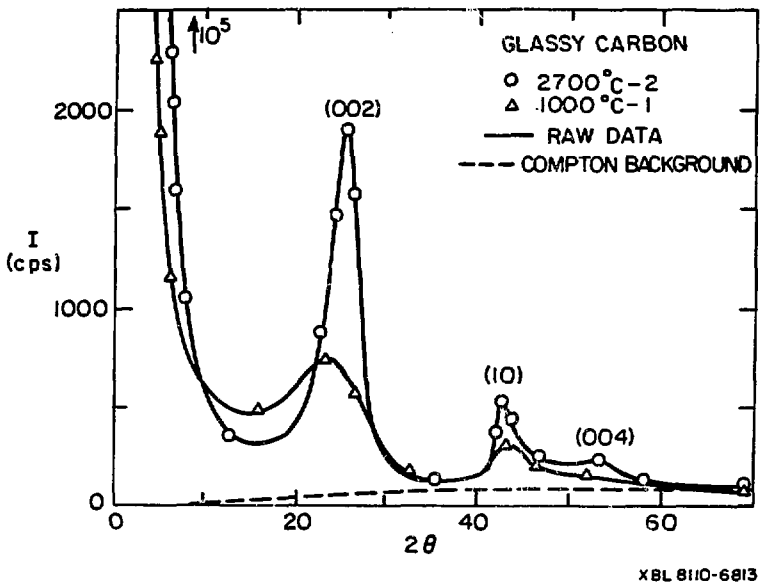
GLASSY CARBON
2700°C-2
1000°C-1
RAW DATA
COMPTON BACKGROUND
(002)
(10)
(004)
10^5
I
(cps)
2000
1000
0
0
20
40
60
2θ
XBL 8110-6813

Fig. 2

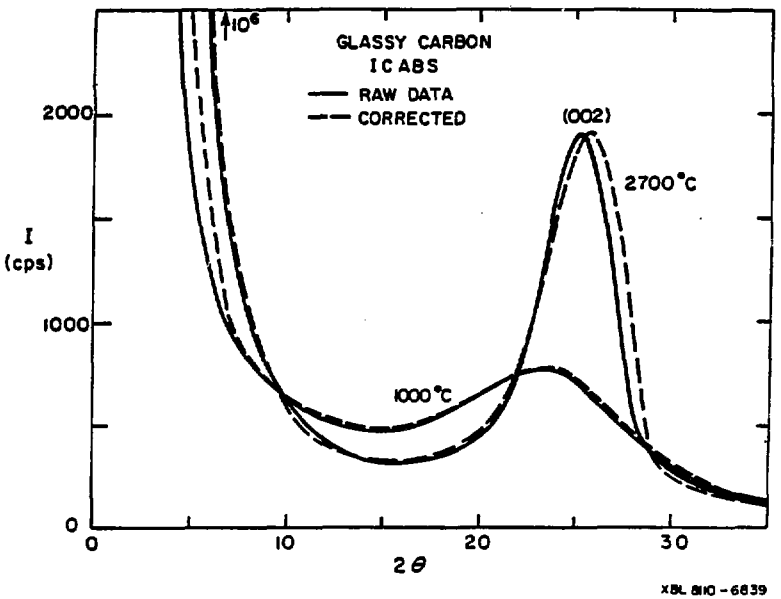
GLASSY CARBON
IC ABS
RAW DATA
CORRECTED
(002)
2700°C
1000°C
10⁶
I
(cps)
2000
1000
0
0
10
20
30
2θ
XBL 8110-6839

Fig. 3

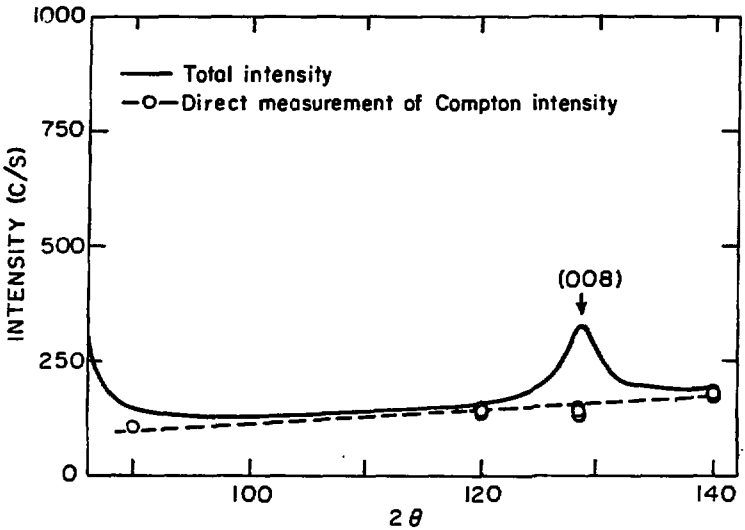

XBL 8012-13461B

Fig. 4

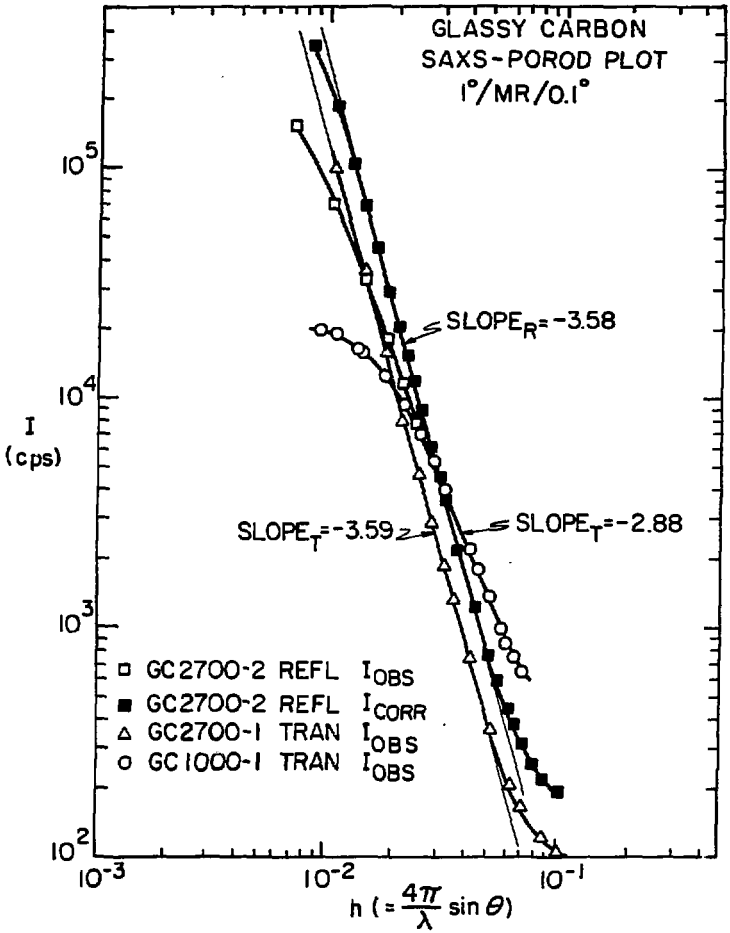

XBL829-6604

Fig. 5

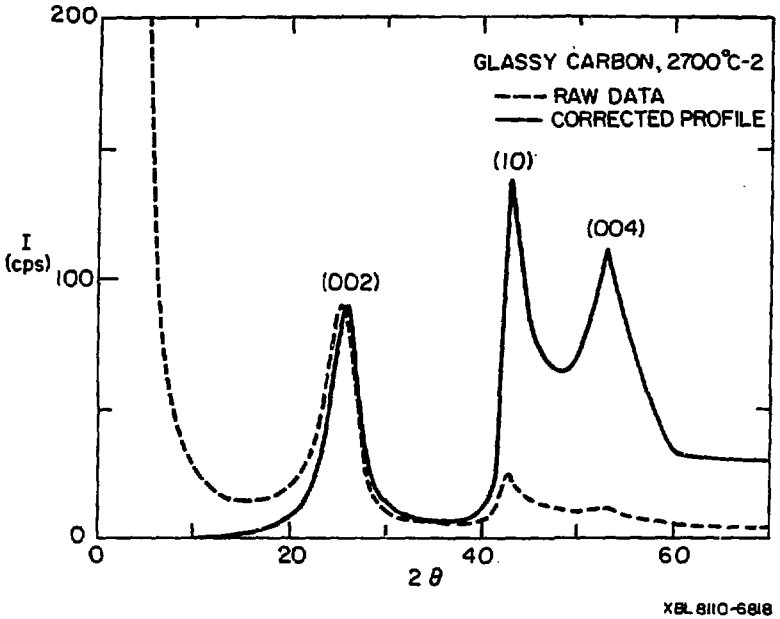
200
100
0
I
(cps)
GLASSY CARBON, 2700°C-2
RAW DATA
CORRECTED PROFILE
(10)
(004)
(002)
0
20
40
60
2θ
XBL 8110-6818

Fig. 6

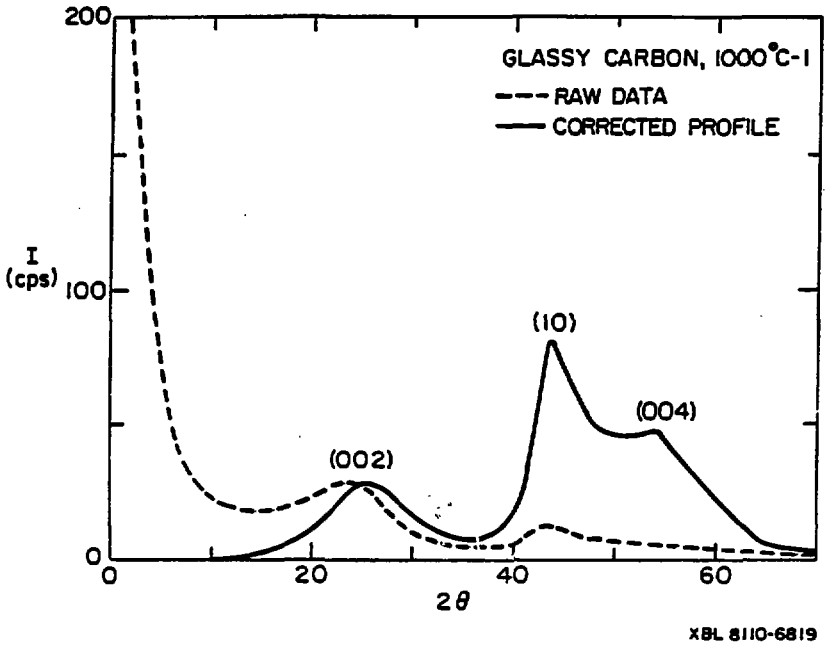
GLASSY CARBON, 1000°C-1
RAW DATA
CORRECTED PROFILE
I
(cps)
200
100
0
(10)
(004)
(002)
0
20
40
60
2θ
XBL 8110-6819

Fig. 7

XBB 777-7454

Fig. 8